Research Article

Characteristics of Wave Reflection for Vertical and Slit Caissons with Porous Structures

Tae-Hwa Jung,[1] Sung-Jae Lee,[2] and Yong-Sik Cho[2]

[1] *Department of Civil Engineering, Hanbat National University, San 16-1, Duckmyoung-dong, Daejeon 305-719, Republic of Korea*
[2] *Department of Civil and Environmental Engineering, Hanyang University, 222 Wangsimni-ro, Seongdong-gu, Seoul 133-791, Republic of Korea*

Correspondence should be addressed to Yong-Sik Cho, ysc59@hanyang.ac.kr

Offshore structures are occasionally located at a relatively deep water region, the outside of breakwater. In this case, these structures may be damaged by the supposition of incident and reflected waves from a vertical breakwater. To prevent the damage, the reflected waves are controlled by installing porous structures at the face of the vertical breakwater. In this study, numerical experiments are carried out to identify the characteristics of wave reflection from the porous structures installing in front of a vertical or slit caisson.

1. Introduction

Offshore structures such as oil buoys or floating structures are sometimes required to be located outside of a breakwater. These structures may be damaged by the reflected waves from a vertical breakwater as well as incident waves. Thus, it is important to reduce the energy of reflected waves from a vertical breakwater to secure the stability of offshore structures. One possible way to reduce reflected waves is dissipating wave energy by adding porous structures at the face of a vertical breakwater.

   Few studies regarding numerical experiments have been paying attention to the wave reflection from a vertical breakwater with a frontally porous structure because of complexities of interaction between porous flow and nonlinear waves. The mechanism of wave energy dissipation and reflection due to a porous structure is not yet clearly understood. Therefore, the energy dissipation efficiency of a permeable structure was assessed by measuring the wave reflection from the breakwater. Sollit and Cross [1] performed the study on wave

reflection and transmission through a porous structure using the linear wave theory and the linearized friction equation for flows in porous media. Following Sollit and Cross [1], several researches were carried out on wave and porous structure interaction [2, 3]. However, these studies were less practical because they assumed linear wave, constant depth, or integrated over the depth. The applicability of numerical study on water waves and porous structures was much improved by adopting the Navier-Stokes equation [4].

In this study, a numerical experiment was carried out to investigate the characteristics of a reflected wave from a porous structure located in front of a slit caisson. For numerical experiment, CADMAS-SURF [5, 6] was used. The irregular wave based on Bretschneider-Mitsuyasu's frequency spectrum was used, and the three-point method was used to decompose the incident and reflected waves.

2. Numerical Model

2.1. Governing Equations

CADMAS-SURF based on the Navier-Stokes equations is composed of the continuity, momentum, VOF, and turbulence equations.

Continuity equation:

$$\frac{\partial \gamma_x u}{\partial x} + \frac{\partial \gamma_z w}{\partial z} = S_\rho. \tag{2.1}$$

Momentum equation:

$$\lambda_v \frac{\partial u}{\partial t} + \frac{\partial \lambda_x uu}{\partial x} + \frac{\partial \lambda_z wu}{\partial z} = -\frac{\gamma_v}{\rho}\frac{\partial p}{\partial x} + \frac{\partial}{\partial x}\left\{\gamma_x v_e\left(2\frac{\partial u}{\partial x}\right)\right\} + \frac{\partial}{\partial z}\left\{\gamma_z v_e\left(\frac{\partial u}{\partial z} + \frac{\partial w}{\partial x}\right)\right\}$$
$$- D_x u + S_v - R_x,$$
$$\lambda_v \frac{\partial w}{\partial t} + \frac{\partial \lambda_x uw}{\partial x} + \frac{\partial \lambda_z ww}{\partial z} = -\frac{\gamma_v}{\rho}\frac{\partial p}{\partial x} + \frac{\partial}{\partial x}\left\{\gamma_x v_e\left(\frac{\partial w}{\partial x} + \frac{\partial u}{\partial z}\right)\right\} + \frac{\partial}{\partial z}\left\{\gamma_z v_e\left(2\frac{\partial w}{\partial z}\right)\right\}$$
$$- D_z w + S_w - R_z - \gamma_v q,$$

(2.2)

where t is the time, x and z are the horizontal and vertical coordinates, u, w are the horizontal and vertical velocity components, ρ is the density of fluid, p is the pressure, v_e is the summation of molecular kinematic viscosity and eddy kinematic viscosity, g is the gravitational acceleration, γ_v is the volume porosity (fraction of the volume of voids over the total volume), γ_x and γ_z are the surface porosity (fraction of the area of voids over the total area) components in the x and z projections, S_ρ, S_u, and S_w are wave generation source, and D_x and D_z are the coefficients for sponge layer.

Using the inertia coefficient C_m, and γ_v, γ_x, and γ_z the inertia force effects from structure, λ_v, λ_x, and λ_z are written as follows:

$$
\begin{aligned}
\lambda_v &= \gamma_v + (1 - \gamma_v)C_m, \\
\lambda_x &= \gamma_x + (1 - \gamma_x)C_m, \\
\lambda_z &= \gamma_z + (1 - \gamma_z)C_m.
\end{aligned}
\tag{2.3}
$$

With the drag coefficient, C_D, the resistance force due to porous media R_x and R_z are defined by the following equations:

$$
\begin{aligned}
R_x &= \frac{1}{2}\frac{C_D}{\Delta x}(1 - \gamma_x)u\sqrt{u^2 + w^2}, \\
R_z &= \frac{1}{2}\frac{C_D}{\Delta z}(1 - \gamma_z)w\sqrt{u^2 + w^2}.
\end{aligned}
\tag{2.4}
$$

Free Surface Equation (VOF)

The VOF method was used to represent the interface boundary between the water and air, known as free surface [7]. The method introduces a volume of fluid function $F(x, z, t)$ to define the fluid region. The physical meaning of F is the fractional volume of a cell occupied by water. A unit value of F corresponds to a cell full of water, and a zero value indicates that the cell contains no water. Cells with F value between zero and one must then contain a free surface. The advection of free surface is represented by a convective equation of F extended for porous media as follows:

$$
\gamma_v \frac{\partial F}{\partial t} + \frac{\partial \gamma_x u F}{\partial x} + \frac{\partial \gamma_z w F}{\partial z} = S_F,
\tag{2.5}
$$

where S_F is a source term for the wave generation source method.

Turbulence Model

In the turbulent model, a closure k-ε turbulence model is adopted. In the closure k-ε turbulence model, the turbulent kinetic energy k and the rate of dissipation of turbulent

kinetic energy ε are defined in (2.6) and (2.7) using the amount of fluctuation $u'; w'$ and derived from the advection-diffusion equation shown in (2.8) and (2.9):

$$k = \frac{1}{2}\left(u'^2 + w'^2\right), \tag{2.6}$$

$$\varepsilon = v\left\{2\left(\frac{\partial u'}{\partial x}\right)^2 + 2\left(\frac{\partial w'}{\partial z}\right)^2 + \left(\frac{\partial w'}{\partial x} + \frac{\partial u'}{\partial z}\right)^2\right\}, \tag{2.7}$$

$$\gamma_v\frac{\partial k}{\partial t} + \frac{\partial \gamma_x u k}{\partial x} + \frac{\partial \gamma_z w k}{\partial z} = \frac{\partial}{\partial x}\left\{\gamma_x v_k\left(\frac{\partial k}{\partial x}\right)\right\} + \frac{\partial}{\partial z}\left\{\gamma_z v_k\left(\frac{\partial k}{\partial z}\right)\right\} + \gamma_v G_s - \gamma_v\varepsilon, \tag{2.8}$$

$$\gamma_v\frac{\partial \varepsilon}{\partial t} + \frac{\partial \gamma_x u \varepsilon}{\partial x} + \frac{\partial \gamma_z w \varepsilon}{\partial z} = \frac{\partial}{\partial x}\left\{\gamma_x v_\varepsilon\left(\frac{\partial \varepsilon}{\partial x}\right)\right\} + \frac{\partial}{\partial z}\left\{\gamma_z v_\varepsilon\left(\frac{\partial \varepsilon}{\partial z}\right)\right\} + \gamma_v C_1\frac{\varepsilon}{k}G_s - \gamma_v C_2\frac{\varepsilon^2}{k}, \tag{2.9}$$

$$G_s = v_t\left\{2\left(\frac{\partial u}{\partial x}\right)^2 + 2\left(\frac{\partial w}{\partial z}\right)^2 + \left(\frac{\partial w}{\partial x} + \frac{\partial u}{\partial z}\right)^2\right\}, \tag{2.10}$$

where the eddy kinematic viscosity v_t and the diffusion coefficient, and v_k and v_ε are described as follows:

$$v_t = \frac{C_\mu k^2}{\varepsilon},$$
$$v_k = v + \frac{v_t}{\sigma_k}, \tag{2.11}$$
$$v_\varepsilon = v + \frac{v_t}{\sigma_\varepsilon}$$

2.2. Boundary Conditions

To treat outgoing waves effectively, two boundary conditions are employed.

Radiation Boundary Condition

Sommerfeld's open boundary condition is employed as follows:

$$\frac{\partial f}{\partial t} + C\frac{\partial f}{\partial x} = 0, \tag{2.12}$$

where f is the wave property such as a mean velocity or mean free surface displacement, and C is the phase velocity. In the case of a regular wave, it is easy to apply because the phase velocity C is known in advance. In the case of irregular waves, however, it is difficult to satisfy a nonreflection condition because the phase velocity C is not clear.

Absorbing Boundary Condition

Because it is difficult to satisfy Sommerfeld's open boundary condition, sponge layer technique, which gradually attenuates wave energy, is used. The attenuation effect is
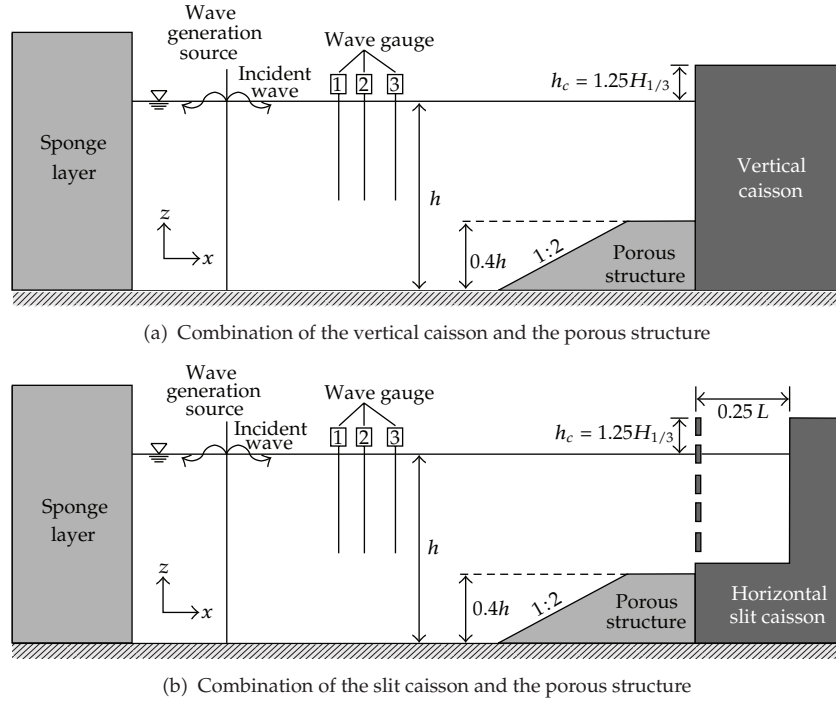
(a) Combination of the vertical caisson and the porous structure

(b) Combination of the slit caisson and the porous structure

Figure 1: Schematic diagram of the numerical wave flume.

represented by $-D_x u$ and $-D_z u$ in the momentum equations of (2.2). Coefficients D_x and D_z are defined as follows:

$$
\begin{aligned}
D_x &= \theta_x \sqrt{\frac{g}{h}} (N+1) \left(\frac{x-x_0}{l} \right)^N, \\
D_z &= \theta_z \sqrt{\frac{q}{h}} (N+1) \left(\frac{x-x_0}{l} \right)^N,
\end{aligned}
\tag{2.13}
$$

where h is the water depth, l and x_0 are the width of a sponge layer and starting point, N is the order of the distribution function, and θ_x and θ_z are the nondimensional coefficients.

3. Numerical Experiments

3.1. Numerical Conditions

The numerical wave flume used in this study is shown in Figure 1. The length of wave flume changed according to the width of the sponge layer, equivalent to $2L$, where L is the incident wave length. The water depth h was set to 0.5 m. In the sponge layer, the wave amplitude decreased exponentially, thus it became small enough to be applied Sommerfeld's radiation condition at the both ends of wave flume. To generate expected target waves unaffected by the sponge layer, the waves are generated inside the computational domain (internal wave generation technique [8]). To analyze wave transformation, three wave gauges were placed

Table 1: Numerical conditions.

Number	Variable	Notation	Range
(1)	Type of wave		Regular wave and irregular wave
(2)	Significant wave height	$H_{1/3}$	2 cm, 3 cm, and 4 cm
(3)	Significant wave period	$T_{1/3}$	1.5 sec., 2.0 sec., and 2.5 sec.
(4)	Type of upright breakwater		Vertical caisson and slit caisson
(5)	Shape of the porous structure		Rectangle, triangle, and trapezoid
(6)	Height of the porous structure		$0.4h$ and $0.8h$
(7)	Water depth	h	$0.5m$
(8)	Wave chamber width	B	$0.25L$

as shown in Figure 2. The distances from the gauges to the porous structure were $1L$, $1L +$ 0.2 m, and $1L + 0.56$ m. That is, the distances between the wave gauges were 0.2 m and 0.36 m. Four combination of the porous structure and the caisson were considered: (1) the vertical caisson only; (2) the vertical caisson and the porous structure; (3) the slit caisson only; (4) the slit caisson and the porous structure. When it comes to the shape of the porous structure, the rectangular, triangular, and trapezoidal shapes were used. The heights of the porous structure were set to $0.4h$ and $0.8h$. The crown height h_c of two kinds of vertical breakwater was set to $1.25H_{1/3}$. Since the ratio of distance of wave chamber to wave length $B/L = 0.25$ is known that it gave the minimum wave reflection [9], a constant value of 0.25 was applied to the wave chamber. In which, the wave chamber means the space between a slit and a vertical wall in the caisson. The significant wave periods of the incident waves were 1.5, 2.0, and 2.5 sec. The significant wave heights of the incident waves were 2.0, 3.0, and 4.0 cm. These conditions are summarized in Table 1.

3.2. Incident Wave

One regular wave and nine irregular waves were used as an incident wave condition. The irregular waves were generated by using following equations:

$$\eta(t) = \sum_{m=1}^{M} a_m \cos(2\pi f_m t - \varepsilon_m),$$

$$u(z,t) = \sum_{m=1}^{M} 2\pi f_m \frac{\cosh k_m(h+z)}{\sinh k_m h} a_m \cos(2\pi f_m t - \varepsilon_m), \qquad (3.1)$$

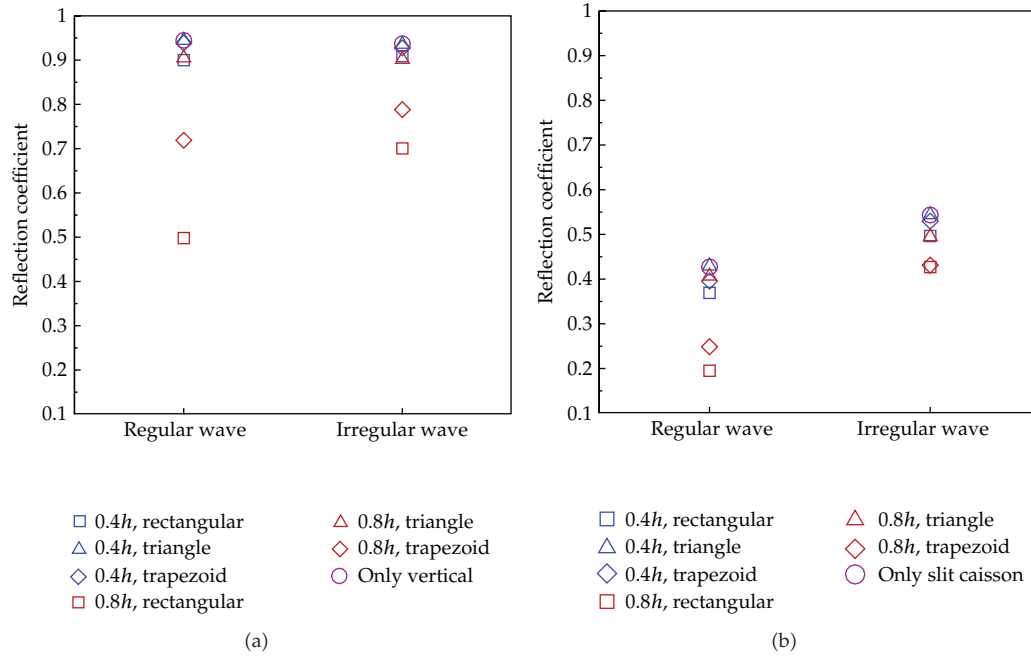$$w(z,t) = \sum_{m=1}^{M} 2\pi f_m \frac{\sinh k_m(h+z)}{\sinh k_m h} a_m \sin(2\pi f_m t - \varepsilon_m),$$

Figure 2: Reflection coefficients of the regular and irregular waves.

where M is a number of frequency, subscript m is mth component, f_m is the corresponding frequency, ε_m is the corresponding random phase angle, k_m is the corresponding wavenumber, and a_m is the corresponding wave amplitude obtained from (3.2):

$$a_m = \sqrt{2S(f)\Delta f}, \tag{3.2}$$

where Δf is the frequency interval, and $S(f)$ is the Bretschneider-Mitsuyasus frequency spectrum given by:

$$S(f) = 0.257H_{1/3}^2 T_{1/3}(T_{1/3}f)^{-5}\exp\left[-1.03(T_{1/3}f)^{-4}\right], \tag{3.3}$$

where f is wave frequency, and $H_{1/3}$ and $T_{1/3}$ are the significant wave height and period, respectively.

3.3. Wave Decomposition

The three-point method suggested by Suh et al. [10] was used to decompose the waves into the incident and reflected waves. A brief description of this method is as follows. Incident and reflected waves can be given by

$$\eta_i(t) = \frac{H_i}{2} \cos(k_i x - \omega t + \phi_i),$$

$$\eta_r(t) = \frac{H_r}{2} \cos(k_r x + \omega t + \phi_r), \tag{3.4}$$

where H is the wave height, k is the wavenumber, ϕ is the random phase angle, and ω is the angular frequency. The surface elevation at the n-point can be expressed as follows:

$$\eta_n(t) = \eta_i(t) + \eta_r(t) = \frac{H_i}{2} \cos(k_i x_n - \omega t + \phi_i) + \frac{H_r}{2} \cos(k_r x_n + \omega t + \phi_r) + e_n(t) \tag{3.5}$$

or

$$\eta_n(t) = X_1 \cos(\omega t - k_i x_n) + X_2 \cos(\omega t - k_r x_n)$$

$$+ X_3 \sin(\omega t - k_i x_n) - X_4 \sin(\omega t - k_r x_n) + e_n(t), \tag{3.6}$$

where x_n is the distance from the first measuring point to the nth location, e_n is error due to signal noise, $X_i (i = 1 \sim 4)$ are unknown coefficients expressed in terms of the height and phase of the incident and reflected waves. The squared error is

$$\varepsilon^2 = \sum_{n=1}^{N} \int_0^T [e_n(t)]^2 dt \tag{3.7}$$

and, the unknowns in (3.6) can be determined by using the least-square method:

$$\frac{\partial \varepsilon^2}{\partial X_j} = 0, \quad j = 1, 2, 3, 4. \tag{3.8}$$

Finally, the incident and reflected wave heights can be calculated using following relation:

$$H_i = \frac{2(X_1 + X_3)}{\cos \phi_i + \sin \phi_i}, \qquad H_r = \frac{2(X_2 + X_4)}{\cos \phi_r + \sin \phi_r}. \tag{3.9}$$
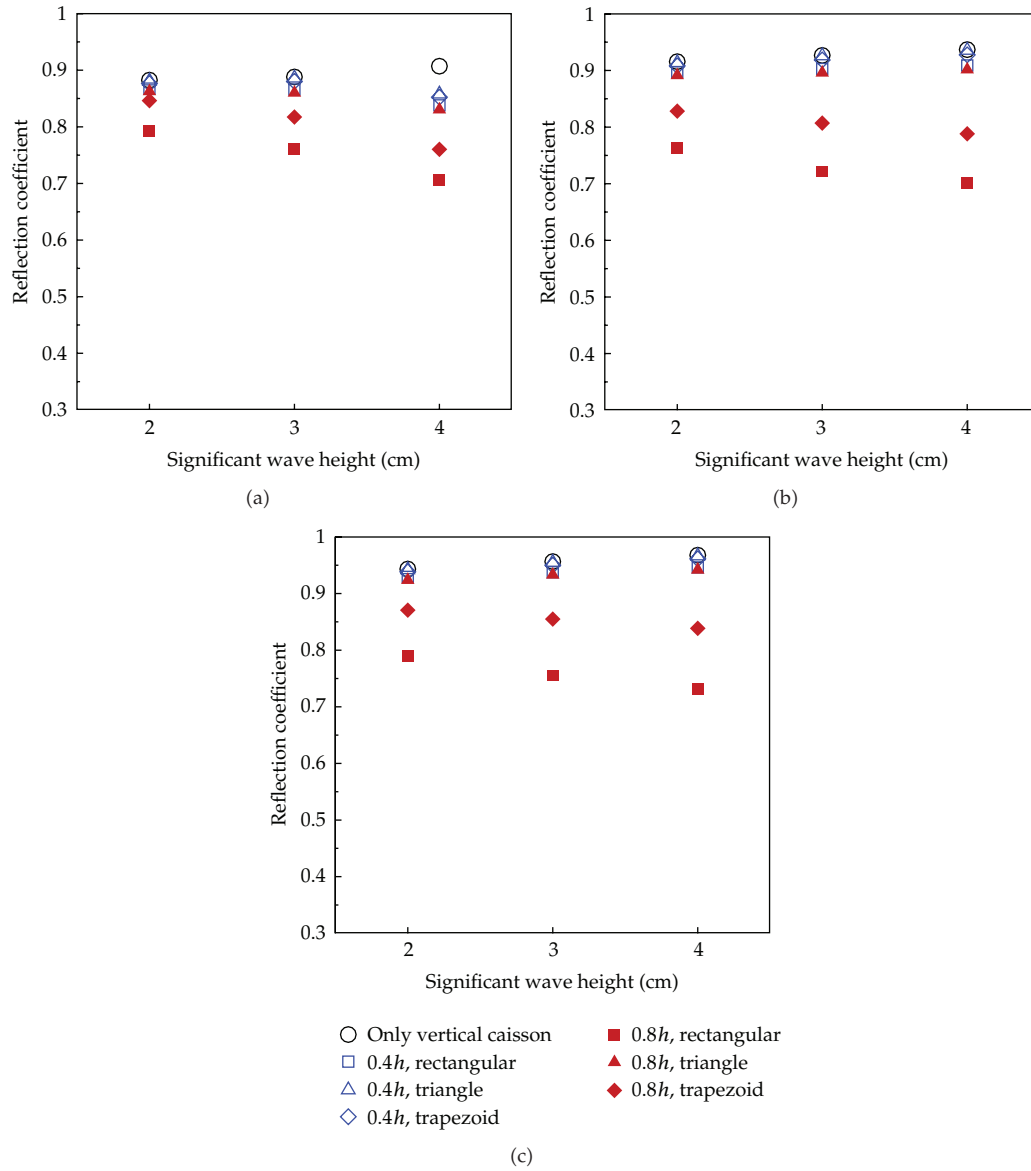
Figure 3: Reflection coefficient for vertical caisson with different significant wave heights.

Since the energies of the incident and reflected waves are proportional to the squares of their heights, the reflection coefficient can be estimated from

$$R = \sqrt{\frac{E_r}{E_i}}, \tag{3.10}$$

where E_i and E_r are the energies of the incident and reflected waves, respectively.
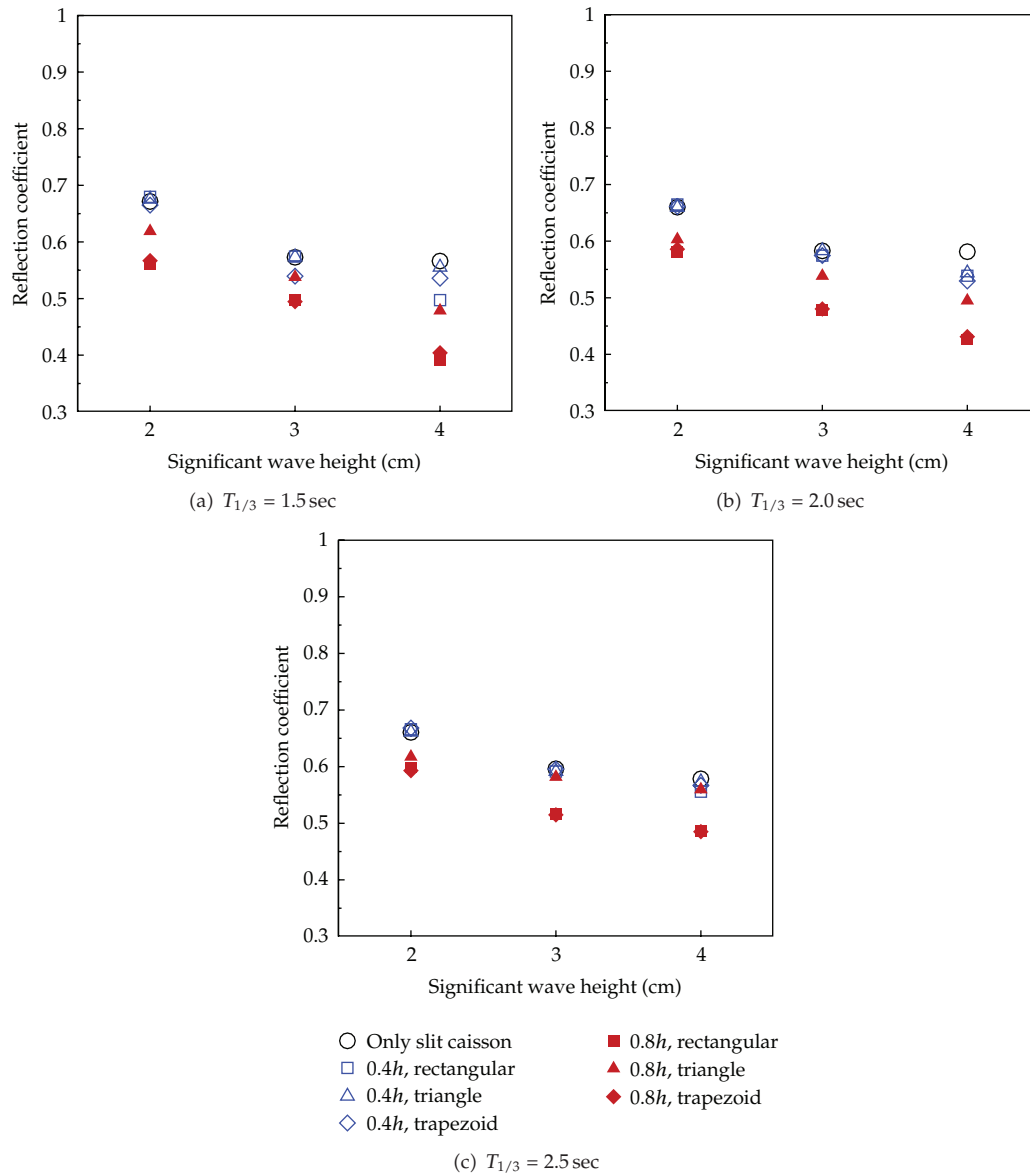
(a) $T_{1/3} = 1.5$ sec

(b) $T_{1/3} = 2.0$ sec

(c) $T_{1/3} = 2.5$ sec

○ Only slit caisson   ■ 0.8h, rectangular
□ 0.4h, rectangular   ▲ 0.8h, triangle
△ 0.4h, triangle   ◆ 0.8h, trapezoid
◇ 0.4h, trapezoid

Figure 4: Reflection coefficient for slit caisson with different significant wave heights.

4. Results and Discussion

Figure 2 showed the reflection coefficients of the regular and irregular waves for the vertical and slit caissons, respectively. The reflection coefficient decreased as the height of the porous structure increased when the porous structure was installed in front of the vertical caisson or the slit caisson. In the case of the regular wave, the reflection coefficient was significantly reduced, whereas the reflection of the irregular waves was slightly reduced. This may be due to fixed width of wave chamber. That is, the width of wave chamber using in the present study referred to the previous study for regular waves. Therefore, it may not be effective
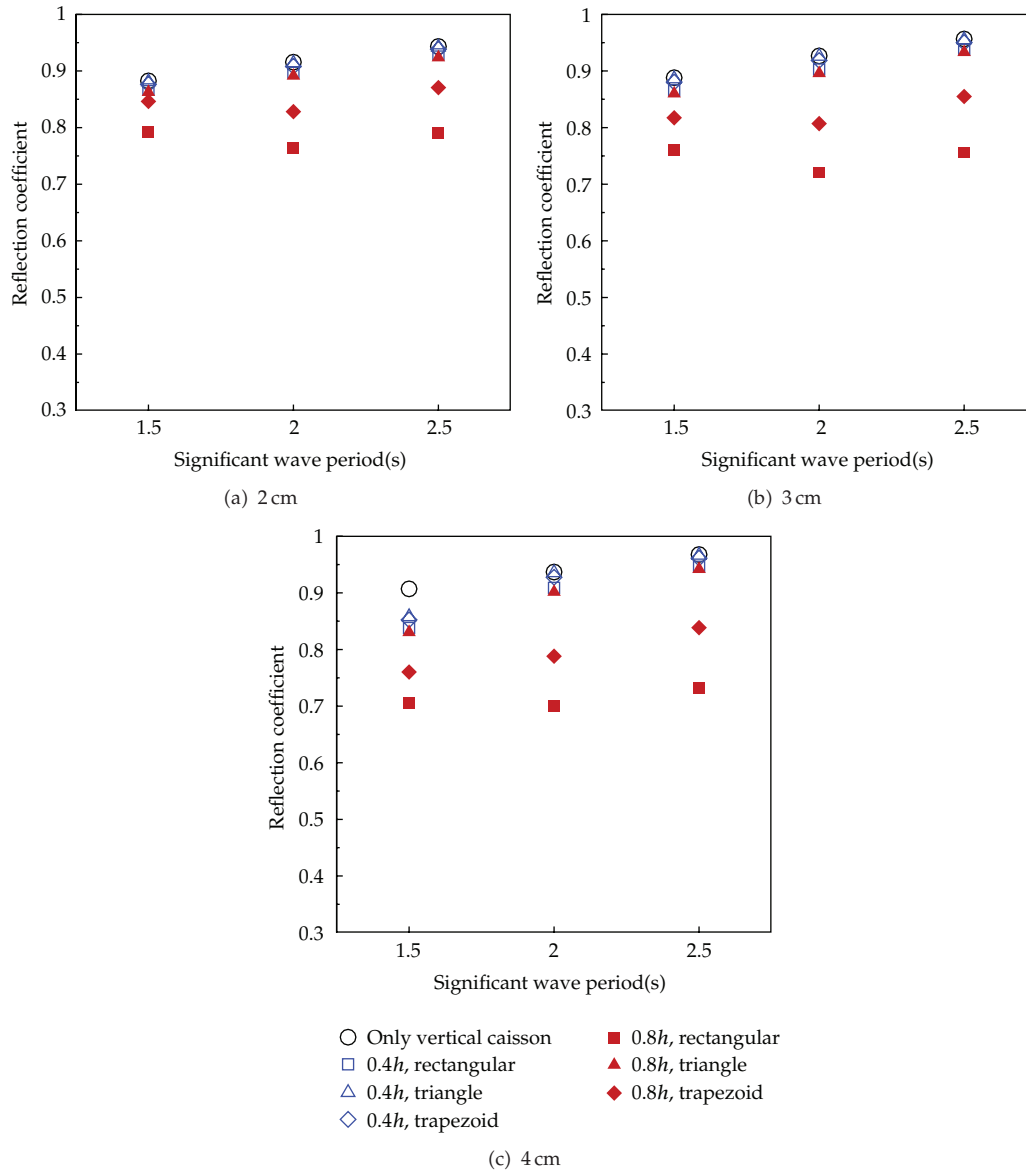
(a) 2 cm

(b) 3 cm

○ Only vertical caisson   ■ 0.8*h*, rectangular
□ 0.4*h*, rectangular   ▲ 0.8*h*, triangle
△ 0.4*h*, triangle   ◆ 0.8*h*, trapezoid
◇ 0.4*h*, trapezoid

(c) 4 cm

Figure 5: Reflection coefficient for vertical caisson with different significant wave periods.

for irregular waves because there are many regular components, and some of them are less affected by the width of wave chamber.

Figures 3 and 4 showed the reflection coefficients for different significant wave heights. It was observed that the reflection coefficient decreased as the height of porous structure increased when the porous structure was located in front of the vertical caisson or the slit caisson. As the height of the significant waves increased, the reflection coefficient decreased. The waves at the slit caisson were more dissipated than those at the vertical caisson.

Figures 5 and 6 showed the reflection coefficients for different significant wave periods. As the height of a porous structure increased, the reflection coefficient decreased
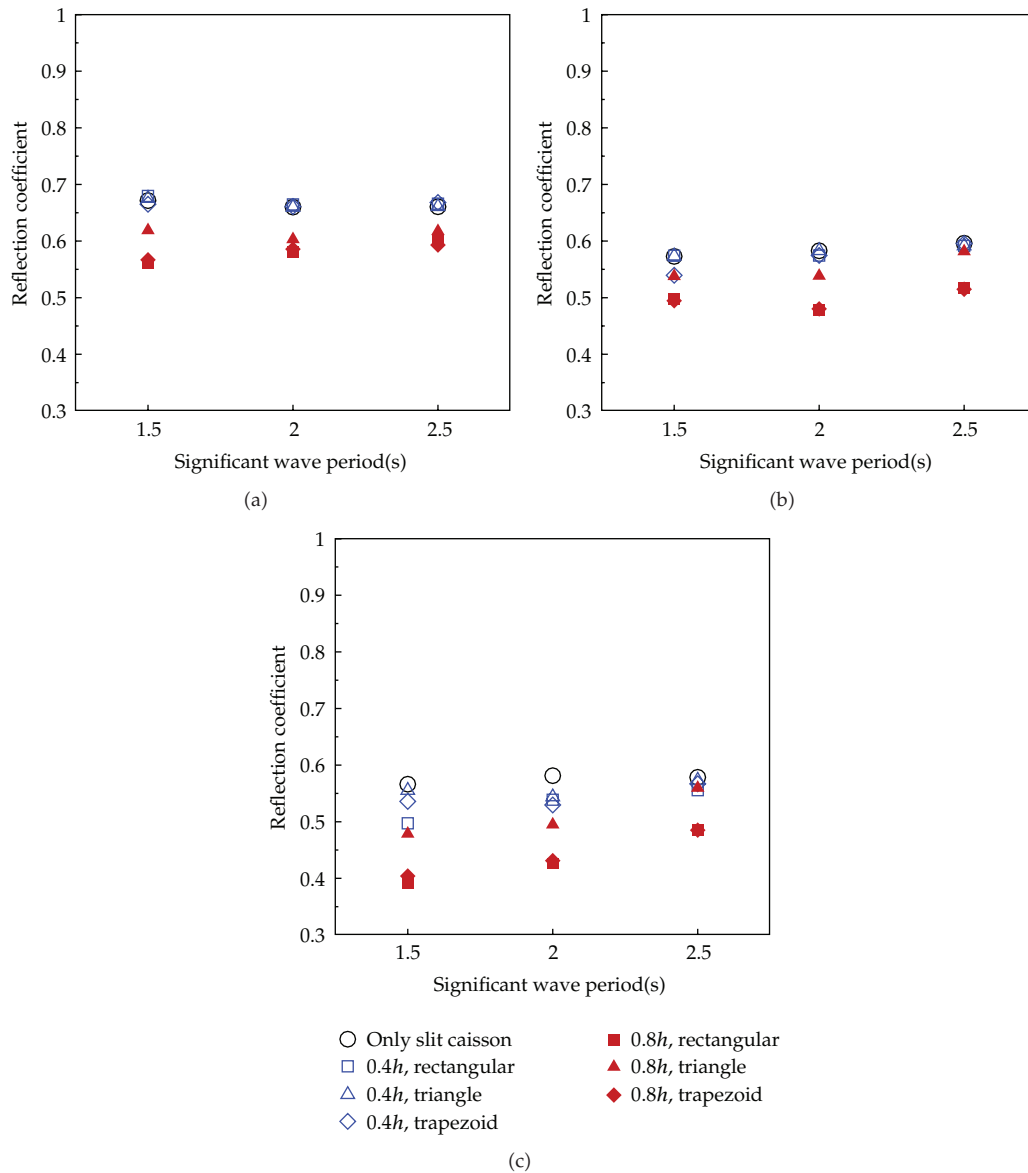
(a)

(b)

(c)

○ Only slit caisson   ■ 0.8*h*, rectangular
□ 0.4*h*, rectangular   ▲ 0.8*h*, triangle
△ 0.4*h*, triangle   ◆ 0.8*h*, trapezoid
◇ 0.4*h*, trapezoid

Figure 6: Reflection coefficient for slit caisson with different significant wave periods.

when the porous structure was located in front of the caisson. The reflection coefficients for a slit caisson were much smaller than those for a vertical caisson. However, the significant wave period rarely affected to the wave reflection. That is, the variation of reflection coefficient due to significant wave period was very small compared to other parameters.

Figures 7 and 8 showed the reflection coefficient for different shapes of porous structure. As the height of porous structure increased, the reflection coefficient decreased. As for the estimated wave coefficients based on the shape of the porous structure, the rectangular and trapezoidal porous structure showed obvious energy dissipation. On the other hand, the
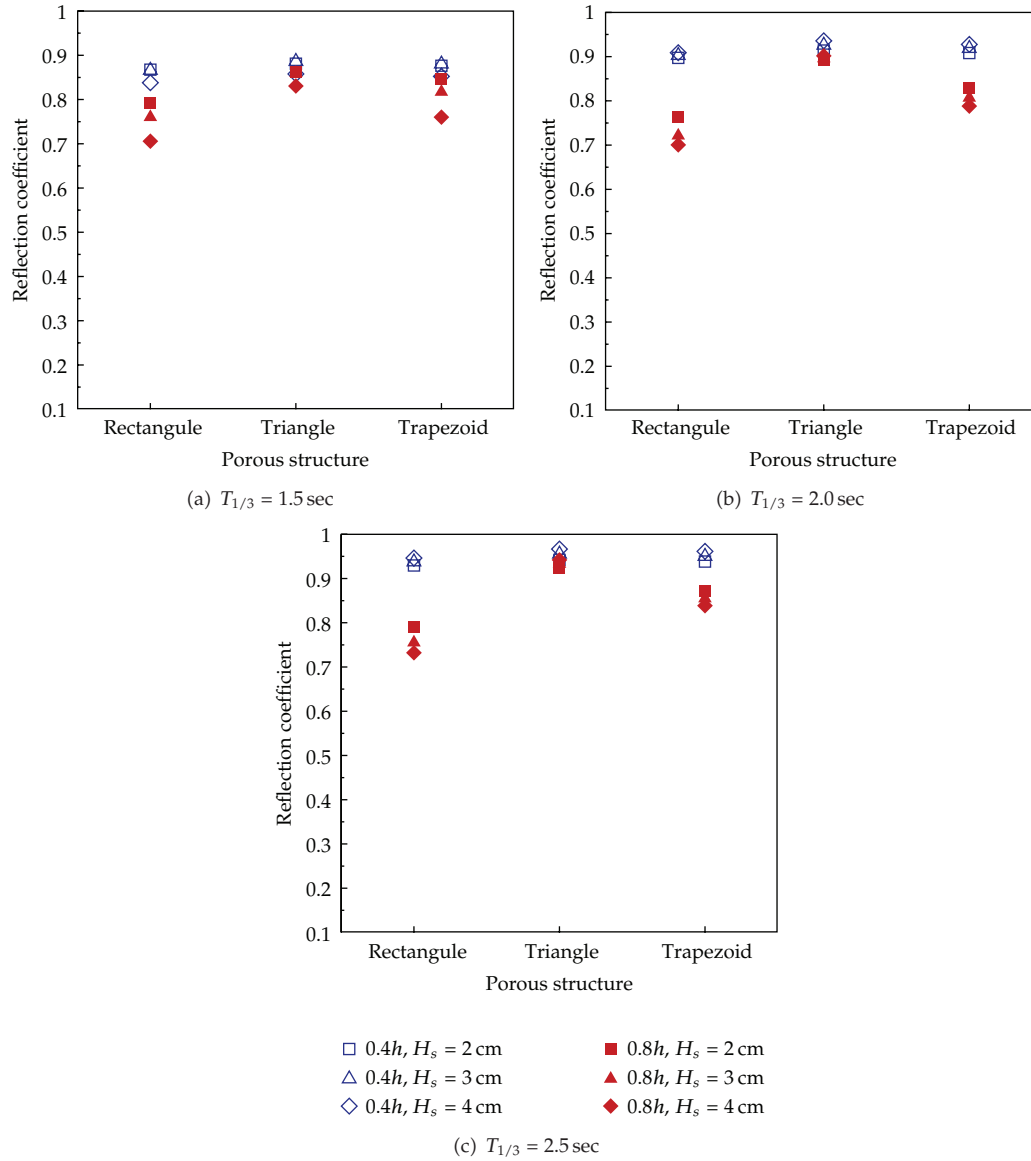
(a) $T_{1/3} = 1.5\,\text{sec}$

(b) $T_{1/3} = 2.0\,\text{sec}$

(c) $T_{1/3} = 2.5\,\text{sec}$

Figure 7: Reflection coefficient for vertical caisson with different shapes of porous structure.

triangular porous structure showed little reduction effect on the slit caisson and almost no reduction on the vertical caisson.

5. Concluding Remarks

In this study, the wave reflection of a vertical and slit caissons with porous structures was analyzed using the number model based on the Navier-Stokes equations. Both of regular and irregular waves were used as incident waves. In the case of regular waves, the reflection coefficient was significantly reduced, whereas the reflection coefficient for irregular
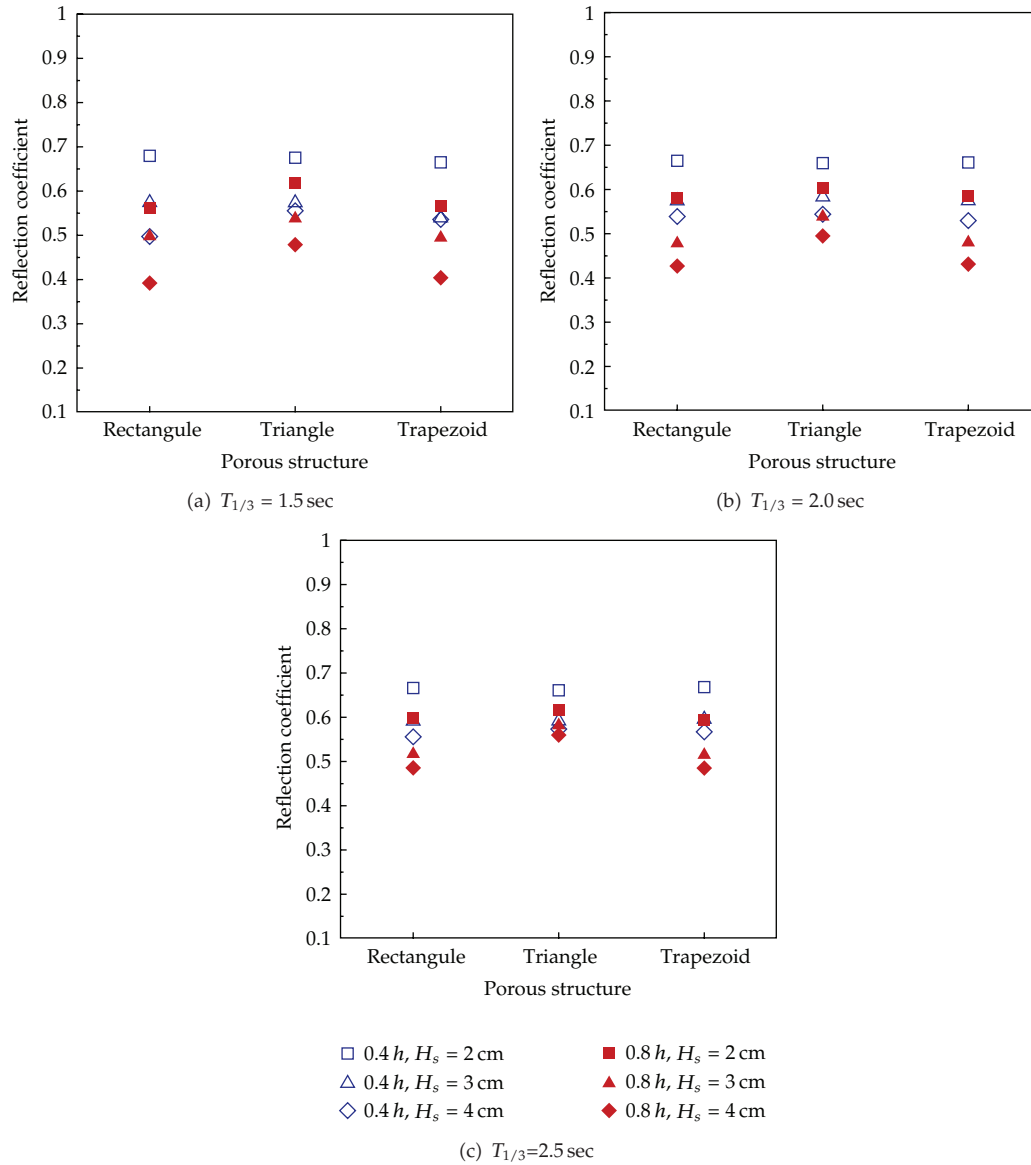
(a) $T_{1/3} = 1.5 \, \text{sec}$

(b) $T_{1/3} = 2.0 \, \text{sec}$

(c) $T_{1/3} = 2.5 \, \text{sec}$

Figure 8: Reflection coefficient for slit caisson with different shapes of porous structure.

waves reduced by a relatively small amount. As the wave height increased, the reflection coefficient decreased for both vertical and slit caissons. The waves were more dissipated at the slit caisson than the vertical caisson. The reflection coefficient was rarely affected by the variation of significant wave period. The rectangular and trapezoidal porous structures showed obvious energy dissipation, whereas the triangular porous structure showed a little reduction effect on the slit caisson and almost no reduction on the vertical caisson. Because porous structure with low height is not able to dissipate wave energy effectively, a proper height is required for efficiency. Although rectangular and trapezoidal porous structures

showed almost same energy dissipation, the trapezoidal structure is more preferred because it has superiority in the workability and stability.

Acknowledgments

References

[1] C. K. Sollit and R. H. Cross, "Wave transmission through permeable breakwaters," in *Proceedings of the 13th International Conference on Coastal Engineering, ASCE*, pp. 1827–1846, 1972.

[2] R. Silva, P. Salles, and A. Palacio, "Linear waves propagating over a rapidly varying finite porous bed," *Coastal Engineering*, vol. 44, no. 3, pp. 239–260, 2002.

[3] H. B. Chen, C. P. Tsai, and J. R. Chiu, "Wave reflection from vertical breakwater with porous structure," *Ocean Engineering*, vol. 33, no. 13, pp. 1705–1717, 2006.

[4] M. F. Karim and T. Tingsanchali, "A coupled numerical model for simulation of wave breaking and hydraulic performances of a composite seawall," *Ocean Engineering*, vol. 33, no. 5-6, pp. 773–787, 2006.

[5] CDIT, *Research and Development of Numerical Channel*, CDIT library, Coastal Development Institute of Technology, 2001.

[6] The Study Group for the Development of CADMAS-SUR, *CADMAS-SURF User's Manual (in Korean)*, 2003.

[7] C. W. Hirt and B. D. Nichols, "Volume of fluid (VOF) method for the dynamics of free boundaries," *Journal of Computational Physics*, vol. 39, no. 1, pp. 201–225, 1981.

[8] J. Larsen and H. Dancy, "Open boundaries in short wave simulations–a new approach," *Coastal Engineering*, vol. 7, no. 3, pp. 285–297, 1983.

[9] M. Fugazza and L. Natale, "Hydraulic design of perforated breakwaters," *Journal of Waterway, Port, Coastal and Ocean Engineering*, vol. 118, no. 1, pp. 1–14, 1992.

[10] K. D. Suh, W. S. Park, and B. S. Park, "Separation of incident and reflected waves in wave-current flumes," *Coastal Engineering*, vol. 43, no. 3-4, pp. 149–159, 2001.